

Neural Network based Robust Adaptive Control for a Variable Stiffness Actuator

Sunghoi Huh

Human-friendly Welfare Robot System
Engineering Research Center (HWRS-ERC), KAIST, Korea
Email: shhuh@ctrsys.kaist.ac.kr

Giovanni Tonietti, Antonio Bicchi

Interdepartmental Research Center "E. Piaggio"
Faculty of Engineering, University of Pisa, Italy
Email: {g.tonietti, bicchi}@ing.unipi.it

Abstract—In this paper we present a robust adaptive controller based on a neural network (NN) for a variable stiffness actuator (VSA). The controller is able to independently set the mechanical stiffness and position at the joint shaft to guarantee robustness with respect to slowly time-varying and unmodeled friction coefficients affecting the dynamics of the actuator. The lumped uncertainties of the VSA including unmodeled dynamics are considered and approximated by a simple NN so that the controlled system is asymptotically stable, and remains effective while process conditions vary. To cope with the reconstruction error of the NN, a sliding mode like additional robust control term is introduced. The proofs for the uniformly ultimately bounded (UUB) and uniform asymptotic (UAS) stabilities for the closed-loop system are provided in detail via Lyapunov theory. Simulation and experimental results are reported in support of both validity and performance of the proposed approach.

Index Terms—Variable Stiffness Actuator, Robust Adaptive Control, Neural Networks, Independent Control of Position and Stiffness.

I. INTRODUCTION

ROBOTS operating in close vicinity to humans present the primary requirement of safety with respect to unwanted collisions with the humans, while the second requirement is their accuracy and rapidity in performing tasks. The classical approach to limit the inherent danger to humans of conventional robot arms is to increase the amount of sensors [15], [16] and to adopt suitable active control strategies (e.g., force/impedance control). However, in practical cases, making rigid arms which behave fast and safely is almost impossible.

Another approach to guarantee limited injury levels for robot arms interacting with humans is to intentionally introduce mechanical compliance in the design [1], [3], [4], [12]. With this measure, researchers tend to dynamically decouple the actuator's rotor inertia from the links whenever an impact occurs. Naturally, compliant transmissions negatively affect performance in terms of increased oscillations and settling time. Accuracy in positioning and stiffness tuning should then be recovered by suitable control policies. Among these, in [1], [3] is investigated the optimal design of mechanisms and controllers for joint actuators of safe and performant robotic manipulators. The Variable Impedance Approach (VIA) is then presented as an innovative solution based on mechanical actuator-transmission systems, that can vary their impedance parameters continuously and in real-time during motion. In particular, it is introduced the idea of using a transmission system with varying stiffness, whose

amount is optimally controlled to increase the performance of the mechanism while satisfying safety constraints. It should be pointed out that, while several mechanisms have been proposed in the robotics literature that can change transmission stiffness to adapt to different tasks (see e.g. [18], [19]), the originality of this approach relies in dynamically controlling transmission stiffness within a single task. In particular, high stiffness is set during low velocity tasks so as to preserve accuracy in positioning, while low stiffness is set for high-velocity tasks, guaranteeing low physical injury in case of impact with a human. A prototype for a 1 d.o.f. variable stiffness mechanism (Variable Stiffness Actuator, VSA) is presented in [2], [3]. The VSA is constituted by two electric motors which are connected to the joint shaft via a mechanical transmission whose stiffness can vary in real-time, and independently, to the position of the joint shaft. The amount of stiffness depends on the relative angular displacement of the two motors. It must be noticed that the dynamic behaviour of the VSA is affected by slowly time-varying friction coefficients at the shafts. These parameters are hard to be modeled, so the need for a control law that adapts itself under such conditions to give reliable performance.

Recently, NNs are widely used as universal approximators in the area of nonlinear mapping and control problems [5], [6], [8], [9], [13], [14], [10], [11], and among them, Radial-Basis Function Networks (RBFNs) can be noticed due to their increased performance despite of the simple structure, constituted of input, output and hidden layers of normalized Gaussian activation functions [5], [9]. Because RBFNs are universal approximators like fuzzy and neural systems [4], RBFNs have been introduced as a viable solution to the multivariate interpolation problem. However, there will be non negligible reconstruction errors if the structure of the RBFN (the number of activation functions in the hidden layer) is not "infinitely rich". These errors inevitably deteriorate the dynamic behaviour and stability of the closed loop system. To minimize the energy of the reconstruction error, sliding-mode-like compensating input terms are widely used, that depend mainly on the bounds of the system uncertainties. In general, these bounds are hard to be correctly estimated, so the control scheme usually adopts overestimated bounds obtained via off-line learning phases.

This paper proposes a robust control approach, aiming at improving performance in controlling position and stiffness at the joint shaft of the VSA. Uncertainties including

unmodeled dynamics which affect the dynamic behaviour of the VSA are estimated using a RBFN, and additional robust control terms are introduced to compensate for the reconstruction error of the network. Both control input and adaptive laws for the weights of the RBFN are established so that the closed-loop system is stable. Detailed proofs for the uniformly ultimately bounded (UUB) and uniform asymptotic (UAS) stabilities for the closed loop system are reported. Finally, simulation and experimental results will highlight the effective performance of the proposed adaptive control approaches compared to a classic PID control.

II. THE VARIABLE STIFFNESS ACTUATOR

In this section we present the design of a compact Variable Stiffness Actuator (VSA), that has been conceived to actuate the joints of robot arms which operate in anthropic environments.

The appearance of the VSA is reported in fig. 1. The actuator consists of two independently controlled brushless DC motors, which are connected to the joint shaft by a timing belt. The belt is tensioned by means of three idle pulleys, connected to the casing by passive elastic elements.

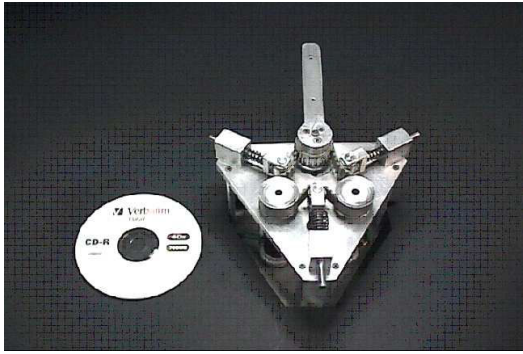


Fig. 1. Appearance of the Variable Stiffness Actuator.

A. Overview of the variable stiffness transmission

The core of the VSA is its torque transmission system (see fig. 2). A timing belt connects the actuators' pulleys to the joint shaft.

Taking into account the mechanism of spring action reported in fig. 3, the contribute at the overall torque acting on the joint q_b generated by the linear spring K_s can be obtained as it follows

$$\phi_{b,a} = F_{b,a} \cos \alpha R = 2K_s R \frac{\bar{h}_{b,a} - h_{b,a}}{h_{b,a}} L_{b,a},$$

where $L_{b,a} = \hat{L}_{b,a} + R(q_b - q_a)$ is the actual length of the belt between the two pulleys ($\hat{L}_{b,a} \geq D$ is the length of the belt in an equilibrium configuration, and R is the radius of the pulleys), while $h_{b,a} = \frac{\sqrt{\hat{L}_{b,a}^2 - D^2}}{2}$ is the active length of the spring ($\bar{h}_{b,a} \geq h_{b,a}$ represents the spring length at rest). Values for these parameters of the VSA are $D = 0.06$ m, $\hat{L}_{b,a} = 0.08$ m, $K_s = 1500$ N/m, $R = 0.015$ m, $\bar{h}_{b,a} = 0.03$ m, and the subscript b, a represents values of the possible pairs (1, 2), (2, m), and (m , 1).

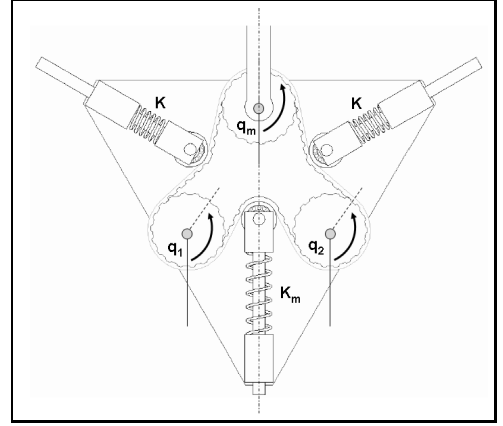


Fig. 2. Design scheme of the variable stiffness transmission. Angular displacements $\delta q_1 = \delta q_2$ for the motor shafts generate only displacements δq_m to the joint shaft. Instead, opposite displacements $\delta q_1 = -\delta q_2$ generate only a variation $\delta \sigma$ for transmission stiffness. Spring of elastic constant K_m is only responsible of the correct tensioning of the belt.

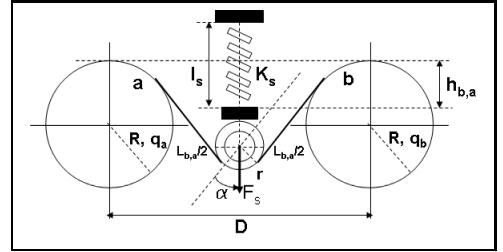


Fig. 3. Particular of the proposed torque transmission system. In this case, stiffness $\sigma_{b,a}$ of the belt that connects the two pulleys b, a varies during motions with the active length $h_{b,a}$ of the spring K_s , in a manner that high/low compressions of the spring generate high/low stiffness.

For simplicity, in these calculations we supposed it holds $r \approx 0$ for the radius of the idle pulley, and that $\bar{h}_{b,a} \approx l_s$, with l_s is the free length of the spring. This stated, the resultant torque τ acting on the joint shaft of the VSA is

$$\tau = \phi_{m,1} - \phi_{2,m} = 2KR \left(\frac{\bar{h}_{m,1} - h_{m,1}}{h_{m,1}} L_{m,1} - \frac{\bar{h}_{2,m} - h_{2,m}}{h_{2,m}} L_{2,m} \right), \quad (1)$$

and for the joint shaft stiffness we obtain

$$\sigma = -\frac{\partial \tau}{\partial q_m} = 2KR \left(\frac{\bar{h}_{m,1} - h_{m,1}}{h_{m,1}} + \frac{\bar{h}_{2,m} - h_{2,m}}{h_{2,m}} \right) - 2KR \left(\frac{\bar{h}_{m,1} L_{m,1}}{4h_{m,1}^3} + \frac{\bar{h}_{2,m} L_{2,m}}{4h_{2,m}^3} \right). \quad (2)$$

It is useful to notice that σ is a monotonically increasing function of the relative displacement of the angular positions of the motors. In particular, it can be shown theoretically that $\sigma \rightarrow +\infty$ for angular values $q_1 = -q_2 \rightarrow \frac{\pi}{2}$, guaranteeing the VSA could perform rigid tasks.

As it will be shown in the following sections, one of the important characteristics of the VSA is that joint stiffness and position can be varied simultaneously and independently adopting suitable nonlinear control policies (see e.g., [3]).

B. Dynamic behaviour of the VSA

The 1 d.o.f. experimental setup we realized is constituted of a rigid link actuated by the VSA. The dynamic behaviour of the system can be formulated, in terms of the mean and

differential displacements $q_s = \frac{q_1+q_2}{2}$, and $q_d = \frac{q_1-q_2}{2}$ of the DC motor angular positions q_1 and q_2 , as

$$\begin{cases} I_R \ddot{q}_s + \beta_1 \dot{q}_s = \Phi_s + \tau_s \\ I_R \ddot{q}_d + \beta_2 \dot{q}_d = \Phi_d + \tau_d \\ J \ddot{q}_m + \beta_m \dot{q}_m + mgL \sin q_m = \phi_{m,1} - \phi_{2,m} - \tau_m \end{cases} \quad (3)$$

where $I_R = 0.0424 \text{ Kg m}^2$ and $J = 0.0625 \text{ Kg m}^2$ are the DC motors and link rotary inertias, respectively, β_1, β_2 , and β_m are (mostly unknowns) friction coefficients, $mg = 9.8 \text{ Kg m/s}^2$ and $L = 0.25 \text{ m}$ are the weight and the length of the link, q_m is the link angular position; $\Phi_s = \frac{\phi_{2,m} - \phi_{m,1}}{2}$, and $\Phi_d = (\phi_{1,2} - \frac{\phi_{2,m} + \phi_{m,1}}{2})$, where $\phi_{1,2}, \phi_{2,m}, \phi_{m,1}$ are the torques generated on the pulleys by the three springs (see section II-A); $\tau_s = \frac{\tau_1 + \tau_2}{2}$, and $\tau_d = \frac{\tau_1 - \tau_2}{2}$, where τ_1, τ_2 are control torques acting on the two motors; τ_m collects external disturbances acting on the link.

III. NN-BASED ROBUST CONTROL APPROACH FOR THE VSA

The aim of this section is to discuss the robust approach we conceived to control the VSA in case of model uncertainties. The control task will be pursued is to control the transmission stiffness σ and the joint shaft position q_m by independently controlling displacements q_s and q_d in (3). The effectiveness of this procedure is highlighted by the fact that, in a steady-state configuration, and in presence of negligible gravitational loads, for the link displacement q_m and transmission stiffness hold respectively $q_m \approx q_s$, and $\sigma \approx \sigma(q_d)$.

The dynamic behaviour of these variables is affected by friction parameters which are slowly time-varying during operations, and modelled as $\beta_i = \bar{\beta}_i + \beta'_i(t)$, where $\bar{\beta}_i$ is the mean-value for the friction coefficient obtained through experiments, and $\beta'_i(t)$ is the behaviour unknown. Moreover, for the purpose of emphasizing compactness of the mechanism, the joint position q_m of the VSA is not equipped with sensors. That implies unknown highly-nonlinear torques Φ_s and Φ_d will affect the dynamic behaviour of positions q_s and q_d during control transients.

Taking into account (3), the dynamic behaviour of q_s and q_d can be expressed in the following state-space form including unmodeled dynamics

$$\begin{cases} \dot{X} = \begin{pmatrix} \dot{x}_1 \\ \dot{x}_2 \\ \dot{x}_3 \\ \dot{x}_4 \end{pmatrix} = \begin{pmatrix} x_2 \\ -I_R^{-1} \bar{\beta}_1 x_2 + I_R^{-1} \tau_s + \Delta_s \\ x_4 \\ -I_R^{-1} \bar{\beta}_2 x_4 + I_R^{-1} \tau_d + \Delta_d \end{pmatrix} \end{cases} \quad (4)$$

where $\Delta_s = I_R^{-1}(-\beta'_1 x_2 + \Phi_s)$ and $\Delta_d = I_R^{-1}(-\beta'_2 x_4 + \Phi_d)$ are unmodeled dynamics, and $X = (x_1, x_2, x_3, x_4)^T = (q_s, \dot{q}_s, q_d, \dot{q}_d)^T$.

If terms Δ_d and Δ_s in (4) are perfectly known, the computed torque controls

$$\begin{cases} \tau_s = I_R(\dot{x}_2^d + I_R^{-1} \bar{\beta}_1 x_2 - \Delta_s + \mathbf{k}_s^T \epsilon_s) \\ \tau_d = I_R(\dot{x}_4^d + I_R^{-1} \bar{\beta}_2 x_4 - \Delta_d + \mathbf{k}_d^T \epsilon_d) \end{cases} \quad (5)$$

in which \dot{x}_2^d and \dot{x}_4^d are reference accelerations for the two motors, guarantee asymptotic convergence to zero for the

tracking errors $\epsilon_s = [q_s^d - q_s, \dot{q}_s^d - \dot{q}_s]^T$ and $\epsilon_d = [q_d^d - q_d, \dot{q}_d^d - \dot{q}_d]^T$, if controller gains $\mathbf{k}_s > 0$ and $\mathbf{k}_d > 0$ are chosen.

Our approach relies in using a computed torque control scheme also in presence of uncertainties, by replacing parameters Δ_s and Δ_d in (5) with suitable estimates $\hat{\Delta}_s$ and $\hat{\Delta}_d$. That gives

$$\begin{cases} \tau_s = I_R(\dot{x}_2^d + I_R^{-1} \bar{\beta}_1 x_2 - \hat{\Delta}_s + \mathbf{k}_s^T \epsilon_s), \\ \tau_d = I_R(\dot{x}_4^d + I_R^{-1} \bar{\beta}_2 x_4 - \hat{\Delta}_d + \mathbf{k}_d^T \epsilon_d). \end{cases} \quad (6)$$

The estimates are computed on-line through a Radial Basis Function Network (RBFN, see Appendix I) whose weights are updated via adaptive laws, and whose inputs are motors' positions and velocities. In the ideal case in which the behaviour for the weights is such that the RBFN perfectly identifies the uncertainties, which means $\hat{\Delta}_s = \Delta_s$ and $\hat{\Delta}_d = \Delta_d$, the controlled system is stable. However, since there will be non-negligible reconstruction errors $\zeta(t)$ between real and approximated values, an additional control component is required to guarantee effective compensation.

Before deriving the feedback control law which includes on-line updates for the weights, and terms for compensation of the reconstruction error, the following definition is useful.

Definition 1 Values for weights \mathbf{W}_s and \mathbf{W}_d that minimize reconstruction errors are defined as

$$\begin{cases} \mathbf{W}_s^* = \operatorname{argmin}_{\mathbf{W}_s \in \Omega_{W_s}} \left[\sup_{\epsilon_s \in \mathbf{U}_c} \|\hat{\Delta}_s(\epsilon_s, \mathbf{W}_s) - \Delta_s\| \right], \\ \Omega_{W_s} = \left\{ \mathbf{W}_s : \|\mathbf{W}_s\| \leq M_{W_s}, M_{W_s} \in \mathbf{R}^+ \right\}, \\ \mathbf{W}_d^* = \operatorname{argmin}_{\mathbf{W}_d \in \Omega_{W_d}} \left[\sup_{\epsilon_d \in \mathbf{U}_c} \|\hat{\Delta}_d(\epsilon_d, \mathbf{W}_d) - \Delta_d\| \right], \\ \Omega_{W_d} = \left\{ \mathbf{W}_d : \|\mathbf{W}_d\| \leq M_{W_d}, M_{W_d} \in \mathbf{R}^+ \right\}, \end{cases} \quad (7)$$

where $\mathbf{U}_c \in \mathbf{R}^2$ is the controllability region, Ω_{W_s} and Ω_{W_d} are bounding sets for the weight vectors \mathbf{W}_s and \mathbf{W}_d respectively.

If we apply control inputs (6) to (4), and using (7), we obtain the following dynamic behaviour for ϵ_s and ϵ_d

$$\begin{cases} \dot{\epsilon}_s = \begin{bmatrix} 0 & 1 \\ -k_{sp} & -k_{sd} \end{bmatrix} \epsilon_s + \begin{bmatrix} 0 \\ 1 \end{bmatrix} \psi_s = \mathbf{A}_s \epsilon_s + \mathbf{B} \psi_s, \\ \dot{\epsilon}_d = \begin{bmatrix} 0 & 1 \\ -k_{dp} & -k_{dd} \end{bmatrix} \epsilon_d + \begin{bmatrix} 0 \\ 1 \end{bmatrix} \psi_d = \mathbf{A}_d \epsilon_d + \mathbf{B} \psi_d, \end{cases} \quad (8)$$

where $\psi_s = (\mathbf{W}_s - \mathbf{W}_s^*)^T \mathbf{Z}_s + \zeta_s - I_R^{-1} \tau_s$, and $\psi_d = (\mathbf{W}_d - \mathbf{W}_d^*)^T \mathbf{Z}_d + \zeta_d - I_R^{-1} \tau_d$, with $\zeta_s = \Delta_s^* - \Delta_s$, and $\zeta_d = \Delta_d^* - \Delta_d$. Vectors \mathbf{Z}_s and \mathbf{Z}_d collect the outputs of the nodes of the NNs' hidden layers (see Appendix I).

In the following we assume that the reconstruction errors ζ_s and ζ_d are bounded, i.e. hold

$$\begin{cases} |\zeta_s| \leq \bar{\zeta}_s, \\ |\zeta_d| \leq \bar{\zeta}_d, \end{cases} \quad (9)$$

where $\bar{\zeta}_s > 0$ and $\bar{\zeta}_d > 0$ are constants. Moreover, because \mathbf{A}_s and \mathbf{A}_d in (8) are Hurwitz matrices, there exist positive definite symmetric matrices \mathbf{P}_s and \mathbf{P}_d that satisfy the following Lyapunov equations

$$\begin{cases} \mathbf{A}_s^T \mathbf{P}_s + \mathbf{P}_s \mathbf{A}_s = -\mathbf{Q}_s, \\ \mathbf{A}_d^T \mathbf{P}_d + \mathbf{P}_d \mathbf{A}_d = -\mathbf{Q}_d, \end{cases}$$

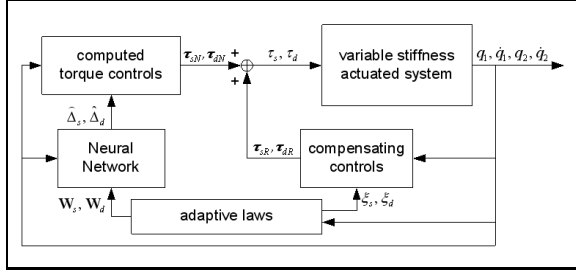


Fig. 4. Conceptual scheme of the proposed control system.

where \mathbf{Q}_s and \mathbf{Q}_d are positive definite matrices.

Theorem 1 The Uniformly Asymptotic Stability (UAS) is guaranteed for all signals in the closed loop system reported in fig. 4, constituted of the VSA's dynamic behaviour (4) controlled by the adaptive computed torque τ_{sN} and compensating controls τ_{sR} as follows

$$\begin{cases} \tau_s = \tau_{sN} + \tau_{sR}, \\ \tau_d = \tau_{dN} + \tau_{dR}, \\ \tau_{sN} = I_R(\dot{x}_2^d + I_R^{-1}\bar{\beta}_1 x_2 - \hat{\Delta}_s + \mathbf{k}_s^T \epsilon_s), \\ \tau_{dN} = I_R(\dot{x}_4^d + I_R^{-1}\bar{\beta}_2 x_4 - \hat{\Delta}_d + \mathbf{k}_d^T \epsilon_d), \\ \tau_{sR} = I_R \xi_s \text{sgn}(\epsilon_s^T \mathbf{P}_s \mathbf{B}), \\ \tau_{dR} = I_R \xi_d \text{sgn}(\epsilon_d^T \mathbf{P}_d \mathbf{B}), \\ \dot{\mathbf{W}}_s = -\gamma_{ws} \epsilon_s^T \mathbf{P}_s \mathbf{B} \mathbf{Z}_s, \\ \dot{\mathbf{W}}_d = -\gamma_{wd} \epsilon_d^T \mathbf{P}_d \mathbf{B} \mathbf{Z}_d, \\ \dot{\xi}_s = \gamma_{\xi s} |\epsilon_s^T \mathbf{P}_s \mathbf{B}|, \\ \dot{\xi}_d = \gamma_{\xi d} |\epsilon_d^T \mathbf{P}_d \mathbf{B}|, \end{cases} \quad (10)$$

where $\gamma_{\xi d} > 0$, $\gamma_{\xi s} > 0$, $\gamma_{ws} > 0$, and $\gamma_{wd} > 0$ are suitable constants.

Proof Here we will prove the UAS for the error ϵ_s , while the UAS of the error ϵ_d can be shown adopting the same procedure.

We define the Lyapunov function

$$V_s(t) = \frac{1}{2} \epsilon_s^T \mathbf{P}_s \epsilon_s + \frac{1}{2\gamma_{ws}} \tilde{\mathbf{W}}_s^T \tilde{\mathbf{W}}_s + \frac{1}{2\gamma_{\xi s}} \tilde{\xi}_s^2, \quad (11)$$

where $\tilde{\mathbf{W}}_s = \mathbf{W}_s - \mathbf{W}_s^*$, and $\tilde{\xi}_s = \xi_s - \xi_s^*$, and, in particular, $\xi_s^* = \bar{\xi}_s$. By using the following equality

$$\frac{1}{2} (\dot{\epsilon}_s^T \mathbf{P}_s \epsilon_s + \epsilon_s^T \mathbf{P}_s \dot{\epsilon}_s) = -\frac{1}{2} \epsilon_s^T \mathbf{Q}_s \epsilon_s + \epsilon_s^T \mathbf{P}_s \mathbf{B} \psi_s, \quad (12)$$

and adopting (9), the derivative of (11) can be computed as follows

$$\begin{aligned} \dot{V}_s(t) &= -\frac{1}{2} \epsilon_s^T \mathbf{Q}_s \epsilon_s + \epsilon_s^T \mathbf{P}_s \mathbf{B} (\tilde{\mathbf{W}}_s \mathbf{Z}_s + \zeta_s - I_R^{-1} \tau_{sR}) \\ &\quad + \frac{1}{\gamma_{ws}} \tilde{\mathbf{W}}_s^T \dot{\tilde{\mathbf{W}}}_s + \frac{1}{\gamma_{\xi s}} \tilde{\xi}_s \dot{\tilde{\xi}}_s \\ &= -\frac{1}{2} \epsilon_s^T \mathbf{Q}_s \epsilon_s + \frac{1}{\gamma_{ws}} \tilde{\mathbf{W}}_s^T (\dot{\mathbf{W}}_s + \gamma_{ws} \epsilon_s^T \mathbf{P}_s \mathbf{B} \mathbf{Z}_s) \\ &\quad + \epsilon_s^T \mathbf{P}_s \mathbf{B} (\zeta_s - I_R^{-1} \tau_{sR}) + \frac{1}{\gamma_{\xi s}} \tilde{\xi}_s \dot{\tilde{\xi}}_s \\ &\leq -\frac{1}{2} \epsilon_s^T \mathbf{Q}_s \epsilon_s + |\epsilon_s^T \mathbf{P}_s \mathbf{B}| \bar{\zeta}_s - \epsilon_s^T \mathbf{P}_s \mathbf{B} I_R^{-1} \tau_{sR} \\ &\quad + \frac{1}{\gamma_{\xi s}} \tilde{\xi}_s \dot{\tilde{\xi}}_s \\ &= -\frac{1}{2} \epsilon_s^T \mathbf{Q}_s \epsilon_s + |\epsilon_s^T \mathbf{P}_s \mathbf{B}| (\bar{\zeta}_s - \xi_s) + \frac{1}{\gamma_{\xi s}} \tilde{\xi}_s \dot{\tilde{\xi}}_s \\ &= -\frac{1}{2} \epsilon_s^T \mathbf{Q}_s \epsilon_s + \frac{1}{\gamma_{\xi s}} \tilde{\xi}_s (\dot{\tilde{\xi}}_s - \gamma_{\xi s} |\epsilon_s^T \mathbf{P}_s \mathbf{B}|) \\ &= -\frac{1}{2} \epsilon_s^T \mathbf{Q}_s \epsilon_s \leq 0, \end{aligned} \quad (13)$$

that proves the function $V_s(t)$ decreases with time to a constant value $V_s(\infty) = \bar{V}_s \neq 0$. The asymptotic convergence to zero of $\epsilon_s(t)$ will be proved adopting the Barbalat's lemma in [7].

After integration of (13) we obtain

$$\int_0^\infty \epsilon_s^T \mathbf{Q}_s \epsilon_s dt \leq 2(V_s(0) - \bar{V}_s) \neq 0,$$

which implies

$$\lim_{t \rightarrow \infty} \epsilon_s(t) = 0.$$

The latter proves the UAS of the signal $\epsilon_s(t)$. \blacksquare

The above theorem guarantees the UAS for the VSA controlled with (10). In practical cases however, the error $\epsilon_s(t)$ reaches high values in the adaptive transient of the task. That could imply high-frequency chattering of controls $\tau_{sR}(t)$, due to the behaviour of variables $\xi_s(t)$ in (10), that commercial actuators cannot physically support. For that reason, in the following theorem the “ σ modification method” [5] will be used to prevent high-frequencies control inputs, while guaranteeing only Uniformly Ultimately Bounded (UUB) stability instead of UAS for the controlled system.

Definition 2 Consider the nonlinear system

$$\begin{cases} \dot{x}(t) = f(x(t), u(t)), \\ y(t) = h(x(t)). \end{cases} \quad (14)$$

We say that $x(t)$ is *uniformly ultimately bounded (UUB)* if there exists a compact set $S \subset \mathbb{R}^n$ such that for all $x(t_0) = x_0 \in S$, there exists $\chi > 0$ and a positive number $\Xi(\epsilon, x_0)$ such that $x(t) < \epsilon, \forall t \geq t_0 + \Xi$.

Theorem 2 The UUB stability is guaranteed for all signals in the closed loop system reported in fig. 4, constituted of the VSA's dynamic behaviour (4) controlled by the adaptive computed torque τ_{sN} and compensating controls τ_{sR} as follows

$$\begin{cases} \tau_s = \tau_{sN} + \tau_{sR}, \\ \tau_d = \tau_{dN} + \tau_{dR}, \\ \tau_{sN} = I_R(\dot{x}_2^d + I_R^{-1}\bar{\beta}_1 x_2 - \hat{\Delta}_s + \mathbf{k}_s^T \epsilon_s), \\ \tau_{dN} = I_R(\dot{x}_4^d + I_R^{-1}\bar{\beta}_2 x_4 - \hat{\Delta}_d + \mathbf{k}_d^T \epsilon_d), \\ \tau_{sR} = I_R \xi_s \text{sgn}(\epsilon_s^T \mathbf{P}_s \mathbf{B}), \\ \tau_{dR} = I_R \xi_d \text{sgn}(\epsilon_d^T \mathbf{P}_d \mathbf{B}), \\ \dot{\mathbf{W}}_s = -\gamma_{ws} (\epsilon_s^T \mathbf{P}_s \mathbf{B} \mathbf{Z}_s + \sigma_{ws} \mathbf{W}_s), \\ \dot{\mathbf{W}}_d = -\gamma_{wd} (\epsilon_d^T \mathbf{P}_d \mathbf{B} \mathbf{Z}_d + \sigma_{wd} \mathbf{W}_d), \\ \dot{\xi}_s = \gamma_{\xi s} (|\epsilon_s^T \mathbf{P}_s \mathbf{B}| - \sigma_{\xi s} \xi_s), \\ \dot{\xi}_d = \gamma_{\xi d} (|\epsilon_d^T \mathbf{P}_d \mathbf{B}| - \sigma_{\xi d} \xi_d), \end{cases} \quad (15)$$

where $\gamma_{\xi d} > 0$, $\gamma_{\xi s} > 0$, $\gamma_{ws} > 0$, $\gamma_{wd} > 0$, $\sigma_{ws} > 0$, $\sigma_{wd} > 0$, $\sigma_{\xi s} > 0$, and $\sigma_{\xi d} > 0$ are suitable constants.

Proof Here we will prove the UUB of the error ϵ_s , while the UUB of the error ϵ_d can be proved following the same procedure.

We define the Lyapunov function

$$V_s(t) = \frac{1}{2} \epsilon_s^T \mathbf{P}_s \epsilon_s + \frac{1}{2\gamma_{ws}} \tilde{\mathbf{W}}_s^T \tilde{\mathbf{W}}_s + \frac{1}{2\gamma_{\xi s}} \tilde{\xi}_s^2, \quad (16)$$

where $\tilde{\mathbf{W}}_s = \mathbf{W}_s - \mathbf{W}_s^*$, and $\tilde{\xi}_s = \xi_s - \xi_s^*$, and, in particular, $\xi_s^* = \bar{\xi}_s$. By using (12), and the inequalities

$$\begin{aligned} \sigma_{ws} \tilde{\mathbf{W}}_s^T \mathbf{W}_s &= \frac{\sigma_{ws}}{2} \left| \tilde{\mathbf{W}}_s \right|^2 + \frac{\sigma_{ws}}{2} \left| \mathbf{W}_s \right|^2 - \frac{\sigma_{ws}}{2} \left| \mathbf{W}_s^* \right|^2 \geq \\ &\frac{\sigma_{ws}}{2} \left| \tilde{\mathbf{W}}_s \right|^2 - \frac{\sigma_{ws}}{2} \left| \mathbf{W}_s^* \right|^2, \\ \sigma_{\xi_s} \tilde{\xi}_s \xi_s &= \frac{\sigma_{\xi_s}}{2} \left| \tilde{\xi}_s \right|^2 + \frac{\sigma_{\xi_s}}{2} \left| \xi_s \right|^2 - \frac{\sigma_{\xi_s}}{2} \left| \xi_s^* \right|^2 \\ &\geq \frac{\sigma_{\xi_s}}{2} \left| \tilde{\xi}_s \right|^2 - \frac{\sigma_{\xi_s}}{2} \left| \xi_s^* \right|^2, \end{aligned} \quad (17)$$

the derivative of the Lyapunov function can be computed as follows

$$\begin{aligned} \dot{V}_s(t) &= -\frac{1}{2} \epsilon_s^T \mathbf{Q}_s \epsilon_s + \epsilon_s^T \mathbf{P}_s \mathbf{B} \left(\tilde{\mathbf{W}}_s \mathbf{Z}_s + \zeta_s - I_R^{-1} \tau_s R \right) \\ &\quad + \frac{1}{\gamma_{ws}} \tilde{\mathbf{W}}_s^T \dot{\mathbf{W}}_s + \frac{1}{\gamma_{\xi_s}} \tilde{\xi}_s \dot{\xi}_s \\ &= -\frac{1}{2} \epsilon_s^T \mathbf{Q}_s \epsilon_s + \epsilon_s^T \mathbf{P}_s \mathbf{B} \left(\tilde{\mathbf{W}}_s^T \mathbf{Z}_s + \zeta_s - I_R^{-1} \tau_s R \right) \\ &\quad + \frac{1}{\gamma_{ws}} \tilde{\mathbf{W}}_s^T \left(-\gamma_{ws} \epsilon_s^T \mathbf{P}_s \mathbf{B} \mathbf{Z}_s - \gamma_{ws} \sigma_{ws} \mathbf{W}_s \right) \\ &\quad + \frac{1}{\gamma_{\xi_s}} \tilde{\xi}_s \left(\gamma_{\xi_s} \left| \epsilon_s^T \mathbf{P}_s \mathbf{B} \right| - \gamma_{\xi_s} \sigma_{\xi_s} \xi_s \right) \\ &\leq -\frac{1}{2} \epsilon_s^T \mathbf{Q}_s \epsilon_s + \left| \epsilon_s^T \mathbf{P}_s \mathbf{B} \right| \left| \tilde{\zeta}_s \right| - \epsilon_s^T \mathbf{P}_s \mathbf{B} I_R^{-1} \tau_s R \\ &\quad + \left| \epsilon_s^T \mathbf{P}_s \mathbf{B} \right| \left| \xi_s \right| - \left| \epsilon_s^T \mathbf{P}_s \mathbf{B} \right| \left| \xi_s^* \right| \\ &\quad - \sigma_{ws} \tilde{\mathbf{W}}_s^T \mathbf{W}_s - \sigma_{\xi_s} \tilde{\xi}_s \xi_s \\ &= -\frac{1}{2} \epsilon_s^T \mathbf{Q}_s \epsilon_s - \sigma_{ws} \tilde{\mathbf{W}}_s^T \mathbf{W}_s - \sigma_{\xi_s} \tilde{\xi}_s \xi_s \\ &\leq -\frac{1}{2} \epsilon_s^T \mathbf{Q}_s \epsilon_s - \frac{\sigma_{ws}}{2} \left(\left| \tilde{\mathbf{W}}_s \right|^2 - \left| \mathbf{W}_s^* \right|^2 \right) \\ &\quad - \frac{\sigma_{\xi_s}}{2} \left(\left| \tilde{\xi}_s \right|^2 - \left| \xi_s^* \right|^2 \right) \\ &= -\frac{1}{2} \epsilon_s^T \mathbf{Q}_s \epsilon_s - \frac{\sigma_{ws}}{2} \left| \tilde{\mathbf{W}}_s \right|^2 - \frac{\sigma_{\xi_s}}{2} \left| \tilde{\xi}_s \right|^2 + \lambda_s, \end{aligned} \quad (18)$$

where $\lambda_s = \frac{1}{2} \left(\sigma_{ws} \left| \mathbf{W}_s^* \right|^2 + \sigma_{\xi_s} \left| \xi_s^* \right|^2 \right)$.

From (18), it can be shown that signals present the following bounds

$$\begin{cases} \left| \epsilon_s \right| \leq \sqrt{\frac{\lambda_s}{\left| \mathbf{Q}_s \right|}}, \\ \left| \tilde{\mathbf{W}}_s \right| \leq \sqrt{\frac{2\lambda_s}{\sigma_{ws}}}, \\ \left| \tilde{\xi}_s \right| \leq \sqrt{\frac{2\lambda_s}{\sigma_{\xi_s}}}, \end{cases} \quad (19)$$

for the induced norm $\left| \mathbf{Q}_s \right| = \max_{x \in \mathbf{R}^2} \frac{\left\| \mathbf{Q}_s x \right\|}{\left\| x \right\|}$. That proves the UUB stability for all signals in the control system. ■

IV. SIMULATION RESULTS

This section reports some simulation results that show the effectiveness of the controls proposed in **Theorem 1** and **Theorem 2** to guarantee enhanced trajectory-tracking performance for the joint displacement $q_s \approx q_m$ of the VSA compared to a classic PID control performance. Sinusoidal references are chosen for joint positions as

$$q_s^d(t) = \pi \sin(\omega t),$$

whose frequency ω changes from π rad/s to 2π rad/s at a particular instant during task execution. That is done to test the controls robustness versus sudden discontinuities of reference's velocity.

Joint stiffness $\sigma(q_d)$ is held constant throughout the entire execution of the task, and equal to the value obtained at

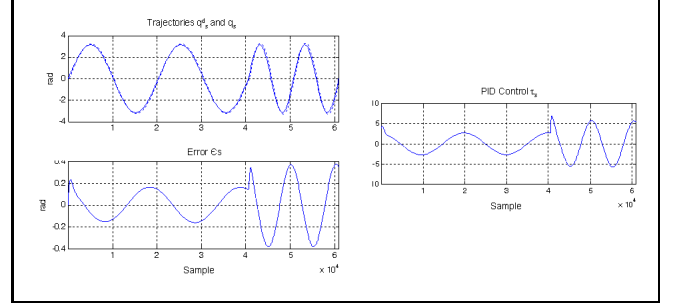


Fig. 5. (Left): reference trajectory q_s^d , resulting q_s trajectory with PID control, and related displacement error ϵ_s . (Right): PID control τ_s .

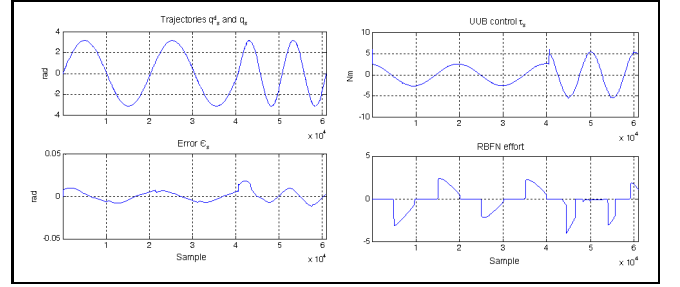


Fig. 6. (Left): reference trajectory q_s^d , resulting q_s trajectory with UUB control, and related displacement error ϵ_s . (Right): UUB control τ_s , and related RBFN effort τ_{sN} during task execution.

the equilibrium configuration corresponding to $q_d = 0$, and $\tau_d = 0$. We will discuss results concerning the independent control for time-varying position and stiffness of the VSA in Section V regarding experimental tests.

Simulations are performed applying controls to the VSA's model (3) in which dynamic parameters have been finely tuned through an extensive experimental campaign (see values reported in section II).

In addition, friction parameters are chosen here to behave as

- $\bar{\beta}_i = 0.5$, $\beta'_i(t) = 0.5 \left(\left| \sin(t) + \sin(0.5t) \right| - 1 \right)$, for $i = 1, 2$.

Results reported in Fig. 5 and Fig. 6 show the VSA's trajectory tracking results obtained with PID control and UUB control respectively. Parameters of the PID control have been tuned experimentally via "trial and error" procedure, and result for both controls τ_s and τ_d as $P = 15$, $I = 1$, and $D = 10$. The UUB control is constituted in particular of a three-layered RBFN with a hidden layer of 5 neurons. Neurons present mean values $\mu_i = -\pi, -\pi/2, 0, \pi/2, \pi$ respectively, while both parameters \mathbf{k}_s and \mathbf{k}_d in (15) are set to 30.

It can be easily noticed that, although the good trajectory tracking performance of the PID, signal ϵ_s increases in that case with reference's frequency, while remains well bounded with UUB control. That is the effect of the RBFN observer that reacts to compensate both reference variations and model uncertainties. Clearly, UUB and PID control performance could still increase through accurate tuning.

Finally, in Fig. 7 it is highlighted that UAS, whose control parameters are set equal to those adopted for UUB control, is obtained through higher frequency controls with respect to

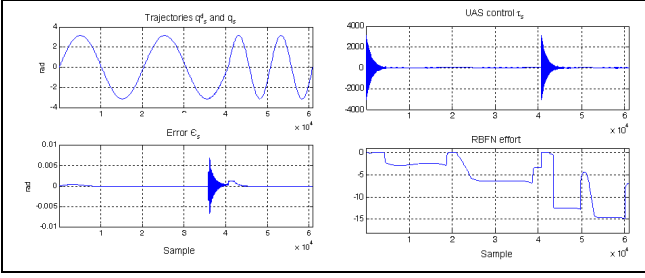


Fig. 7. (Left): reference trajectory q_s^d , resulting q_s trajectory with UAS control, and related displacement error ϵ_s . (Right): UAS control τ_s , and related RBFN effort τ_{sN} during task execution.

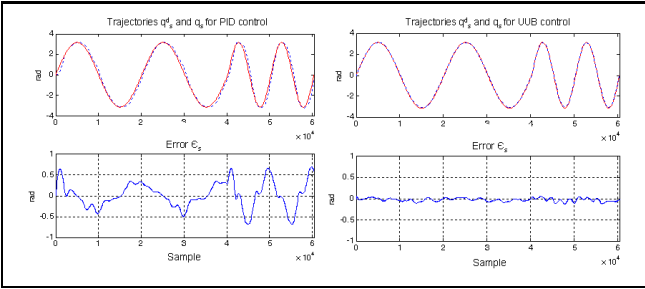


Fig. 8. (Left): reference trajectory q_s^d , resulting q_s trajectory with PID control, and related displacement error ϵ_s . (Right): reference trajectory q_s^d , resulting q_s trajectory with UUB control, and related displacement error ϵ_s .

those for UUB (see comments on Section III). That implies the UUB control is more viable for implementation in our experimental testbed.

V. EXPERIMENTAL RESULTS

This section reports results obtained through trajectory-tracking experiments for the VSA controlled with both the PID and the UUB control.

The first results, which show the trajectory-tracking at constant stiffness and sinusoidal position reference, are reported in Fig. 8-(Left) and Fig. 8-(Right) for PID and UUB control respectively. It can be noticed that results comply to those reported in Section IV, denoting worst performance of the PID with respect to UUB control.

An important characteristic of the VSA is that velocity and stiffness at the joint shaft can be controlled independently during task execution. In particular, in [1], [3] it is highlighted that optimal performance under safety constraints for a variable stiffness mechanism can be guaranteed allowing the mechanical stiffness to vary accordingly to the “fast-and-soft&slow-and-stiff” paradigm, i.e. stiffness reaches higher values for low velocities, while decreases for faster movements. To this purpose, results concerning the independent tracking of velocity (i.e., \dot{q}_s) and stiffness (i.e., q_d) at the joint shaft of the VSA are reported in Fig. 9 and Fig. 10 for PID and UUB control respectively. Even though both controls show good tracking behaviour for joint shaft velocity, stiffness control with UUB presents a distinguishable performance against that of PID. In fact, PID is not able to effectively react to nonlinear disturbances acting on the dynamics of the DC motors. These disturbances are extremely time-varying, depending in particular to the

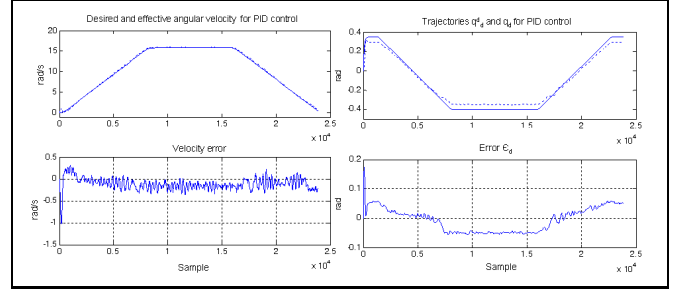


Fig. 9. (Left): reference trajectory \dot{q}_s^d , resulting \dot{q}_s trajectory with PID control, and related velocity error ϵ_s . (Right): reference trajectory q_d^d , resulting q_d trajectory with PID control, and related displacement error ϵ_d .

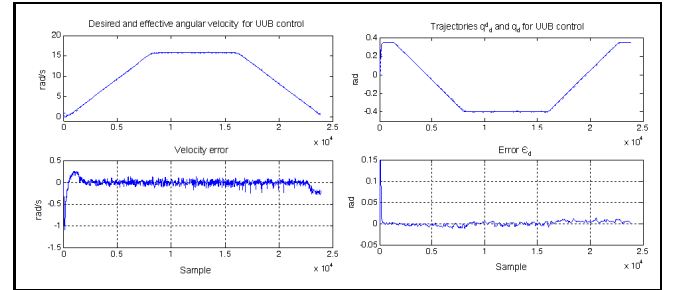


Fig. 10. (Left): reference trajectory \dot{q}_s^d , resulting \dot{q}_s trajectory with UUB control, and related velocity error ϵ_s . (Right): reference trajectory q_d^d , resulting q_d trajectory with UUB control, and related displacement error ϵ_d .

stiffness characteristic of the transmission that is varied during the task.

The UUB control can instead adaptively tune the parameters while guaranteeing good performance in such situations. In Fig. 11 are reported controls τ_{sN} , τ_{dN} of the NNs, and the compensating control efforts τ_{sR} , τ_{dR} varied during the task.

VI. CONCLUSION

The independent control of velocity and stiffness for a variable stiffness actuator has been obtained through design of a RBFN-based robust control. The closed-loop system has been shown analytically to be stable in presence of nonlinear and time-varying uncertainties affecting the dynamic behaviour of the actuator. In particular, it has been pointed out that a control that guarantee bounded stability is preferable for implementation in an experimental testbed, even though asymptotically stable control theoretically shows perfect tracking performance. Finally, simulation and experimental results highlight the effective performance of the proposed control compared to that of a classic PID control.

APPENDIX I

RADIAL BASIS FUNCTION NETWORKS

The radial-basis function network (RBFN) presents inputs, outputs, and hidden layers (nodes) of normalized Gaussian activation functions. A schematic diagram of the RBFN is shown in Fig. 12.

The output z_i of the i -th node is computed as follows

$$z_i(\mathbf{X}_{rb}) = \frac{\exp[-\|\mathbf{X}_{rb} - \mathbf{m}_i\|^2/2\mu_i]}{\sum_{k=1}^l \exp[-\|\mathbf{X}_{rb} - \mathbf{m}_k\|^2/2\mu_k]},$$

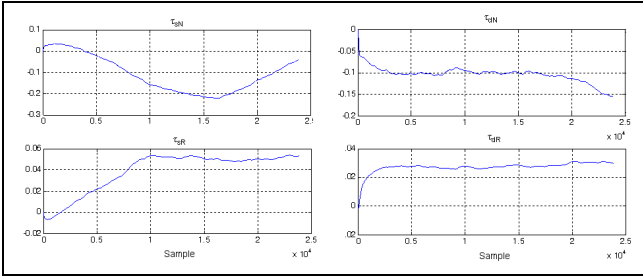


Fig. 11. (Left): controls τ_{sN} and τ_{sR} resulting from the trajectory-tracking experiment reported in Fig. 10-Left. (Right): controls τ_{dN} and τ_{dR} resulting from the trajectory-tracking experiment reported in Fig. 10-Right.

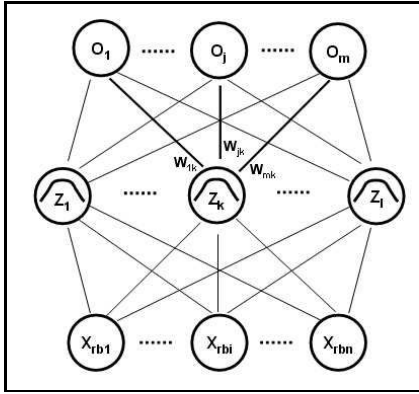


Fig. 12. Schematic diagram of a three-layered Radial Basis Function Network (RBFN).

where l is the number of hidden nodes, $\mathbf{X}_{rb} = (x_{rb,1}, x_{rb,2}, \dots, x_{rb,n}) \in \mathbb{R}^n$ is the input vector, \mathbf{m}_i and μ_i are respectively the center and width of the i -th activation function. The j -th output o_j of the RBFN is defined as a weighted sum of the hidden layer outputs, i.e.

$$o_j = \sum_{k=1}^l w_{jk} z_k = \mathbf{W}_j^T \cdot \mathbf{Z}$$

where $\mathbf{W}_j \in \mathbb{R}^l$ collects weights w_{jk} , and $\mathbf{Z} \in \mathbb{R}^l$ collects the outputs of the nodes. The output of the RBFN is $\mathbf{o} = (o_1, o_2, \dots, o_m)^T \in \mathbb{R}^m$.

Parameters of the RBFN such as weights, center vectors, and widths of the activation functions, can be updated on-line adopting suitable adaptive laws, aiming at guaranteeing asymptotic convergence to zero of the reconstruction error $\zeta(t) = \mathbf{y}(t) - \mathbf{o}(t)$, where $\mathbf{y}(t)$ collects output references [6].

REFERENCES

- [1] A. Bicchi, and G. Tonietti, "Fast and 'soft-arm' tactics," IEEE Robotics and Automation magazine, June, 2004, pp.22-33.
- [2] A. Bicchi, G. Tonietti, and R. Schiavi. "Safe and Fast Actuators for Machines Interacting with Humans". In Proc. of the 1st Technical Exhibition Based Conference on Robotics and Automation, TEXCRA2004, November 18-19, TEPIA, Tokyo, Japan, 2004.
- [3] G. Tonietti, R. Schiavi, and A. Bicchi, "Design and control of a variable stiffness actuator for safe and fast physical human/robot interaction", In Proc. of IEEE Int. Conf. on Robot. and Autom., 2005, pp.526-531.
- [4] G. Pratt and M. Williamson, "Series elastic actuators," In Proc. of IEEE/RSJ Int. Conf. on Intel. Robot. and Syst., 1995, pp.399-406.

- [5] S.H.Huh, "Nonlinear uncertainty observer for AC motor control using the radial basis function networks," IEE Proc.-Control Theory and Appl., vol. 151, no. 3, pp. 369-375, May 2004.
- [6] C.T.Lin, C.S.Lee, Neural fuzzy systems, Prentice Hall, Upper Saddle River, NJ, 1996, pp.328-330.
- [7] J.E.Slotine, W.Li, Applied nonlinear control, Prentice Hall, 1991.
- [8] C.H.Tsai, H.Y.Chung, F.M.Yu, "Neuro-sliding mode control with its applications to seesaw systems," IEEE Trans. Neural networks, vol. 15, no. 1, Jan. 2004, pp.124-134.
- [9] J.H.Park, S.H.Huh, S.H.Kim, S.J.Seo, and G.T.Park, "Direct adaptive controller for nonaffine nonlinear systems using self-structuring neural networks," IEEE Trans. Neural networks, vol. 16, no. 2, Mar. 2005, pp.414-422.
- [10] W.Chatlatanagulchai, P.H.Meckle, "Motion control of two-link flexible-joint robot with actuator nonlinearities using backstepping and neural network," In Proc. of IEEE/RSJ Int. Conf. on Intel. Robot. and Syst., 2005.
- [11] F.Abdollahi, H.A.Talebi, and R.V.Patel, "A stable neural network-based observer with application to flexible-joint manipulator," IEEE Trans. Neural networks, vol. 17, no. 1, Jan. 2006, pp.118-129.
- [12] M.Zinn, and B.Roth, "A new actuation approach for human friendly robot design," The International Journal of Robotics Research, vol. 23, no. 4-5, Apr.-May, 2004, pp.379-398.
- [13] C.M.Lin, Y.F.Peng, and C.F.Hsu, "Robust cerebellar model articulation controller design for unknown nonlinear systems," IEEE Transactions on Circuits and Systems, vol. 51, no. 7, Jul. 2004, pp.354-358.
- [14] R.J.Way, "Total sliding-mode controller for PM synchronous servo motor drive using recurrent fuzzy neural network," IEEE Trans. Indus. Electr., vol. 48, no. 5, Oct. 2001, pp.926-944.
- [15] E. Cheung and V. Lumelsky, "Proximity sensing in robot manipulator motion planning: System and implementation issues," IEEE Trans. Robot. Automat., no. 5, pp. 740-751, 1989.
- [16] H. Iwata, H. Hoshino, T. Morita, and S. Sugano, "Force detectable surface covers for humanoid robots," in Proc. IEEE/ASME Int. Conf. Advanced Intell. Mechatronics, Como, Italy, July 8-11, 2001, pp. 1205-1210
- [17] J.K. Salisbury, Kinematic and Force Analysis of Articulated Hands, Ph.D. thesis, Stanford University, Stanford, CA, May 1982.
- [18] T. Morita and S. Sugano, "Design and development of a new robot joint using a mechanical impedance adjuster," in Proc. IEEE Int. Conf. on Robotics and Automation, 1995, pp. 2469-2475.
- [19] M. Okada and Y. Nakamura, "Development of the cybernetic shoulder - a three-dof mechanism that imitates biological shoulder motion," in Proc. IEEE/RSJ Int. Conf. on Intelligent Robots and Systems, 1999, pp. 453-548.